MAXIMIZING THE TWIST OF COLD FORMED GLAZING°

AUSTIN BENSEND, PE, SE

Realization of architectural vision is driving the advancement of glazing materials and analysis. One realm where this is especially apparent is in the push to achieve freeform glazed surfaces of greater degrees of anticlastic curvature. Often these surfaces are achieved in construction by elastically deforming flat glass into the desired surface geometry by twisting it out of plane. However, the ability to deform the glass in this manner is limited in large part by strength and stability.

Through recent research, Enclos has uncovered some key strategies to maximization of cold warping, as limited by snap-through buckling due to warping and as limited by strength of the glass. The magnitude of twist achieved by elastic deformation of flat glass can be maximized primarily by reducing the short dimension of glass. The general approach to achieving maximum twist is to find the smallest acceptable width dimension for glazing, and then find the required thickness to minimize buckling and resist applied loads, while ensuring thickness is not excessive such that glass stresses due to warping limit the twist magnitude.

Increased twist angle and reduced thickness can simultaneously be realized without compromising the snap-through buckling performance simply by reducing the short dimension of the glass. A secondary benefit of reduction of the short dimension for a lite supported along its perimeter is that the thickness required to resist transverse loads is also reduced. This is because the reduced span results in an increased capacity. Additionally, the internal stresses that arise from enforced torsional deformation of the glass are less with relatively thinner glass.

OBJECTIVE

The objective of the research was to identify the theoretical upper bound of the magnitude of achievable twist, θ, on a single lite of four-side supported, fully tempered glass, as limited by buckling and strength. The variables considered were glass thickness, t; short dimension, B; long dimension, L; and twist, θ. In order to compare specimens of different lengths, twist is expressed as twist per length, θ, which was optimized. Although the glass is twisted out of plane, each edge is held straight such that the perimeter supports are linear along each edge, as seen in Figure 1.

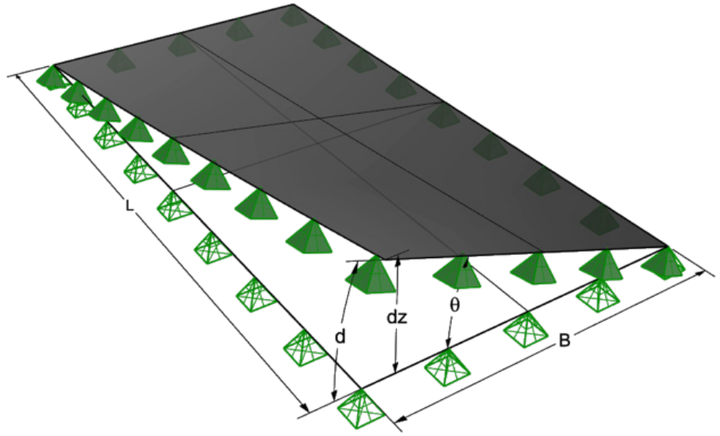

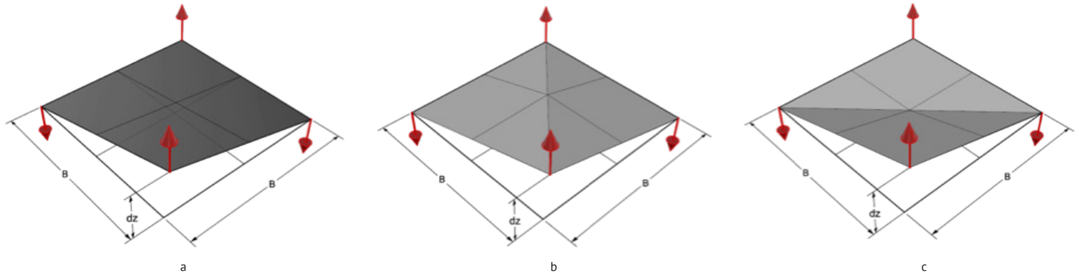

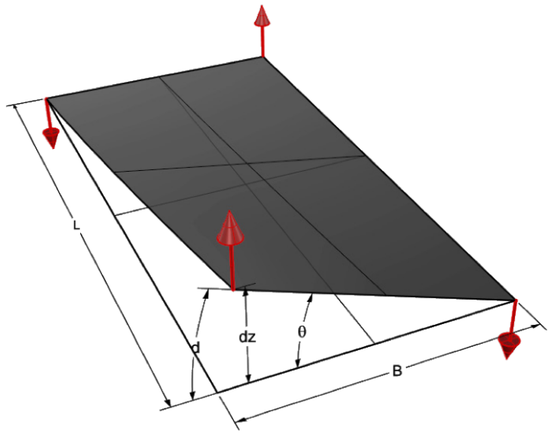

FIGURE 1
Edge support condition and variable definitions for twist optimization problem.

FIGURE 2
Approximate pre- and post-buckled shapes for square, point-supported piece.

FIGURE 3
Twist angle, corner displacement, and arc length.

BACKGROUND

SURFACE BUCKLING OF GLASS IN TORSION

Buckling of a thin rectangular plate is defined as the onset of a bifurcation of a twisted surface as twist is increased, such as shown in Figure 2a. Twisting beyond this point of buckling, alternate modes of the shape may exist in the form of bent rather than twisted shapes, as seen in Figure 2b and 2c. Previously, buckling has been thought to occur at a constant ratio, alpha, shown in the equation below:

(3)

$$\alpha = \left(\frac{d}{t}\right) \cdot \left(\frac{B}{L}\right)$$

This relationship is expressed for both large and small magnitudes of rotation by replacing global displacement, d_z with the arc length, *d* as the glass is twisted out of plane as shown in Figure 3.

SPECIMEN	ASPECT RATIO 'a' [L/B]	SHORT DIMENSION 'B' [MM]	LONG DIMENSION 'L' [MM]	THICKNESS 't' IN FEA MODELS [mm]	THICKNESS 't' AS TESTED [mm]
A	1.00	1524	1524	4.57	4.67
B	1.00	1524	1524	5.56	5.71
C	1.00	1524	1524	9.02	9.37
D	1.50	1524	2286	4.57	4.67
E	1.50	1524	2286	5.56	5.66
F	1.50	1524	2286	9.02	9.55
G	2.00	1524	3048	4.57	4.67
H	2.00	1524	3048	5.56	5.66
I	2.00	1524	3048	9.02	9.50
J	2.40	1524	3658	4.57	4.67
K	2.75	1524	4191	5.56	5.58
L	2.75	1524	4191	9.02	9.35

TABLE 1
Specimens tested previously by Enclos.

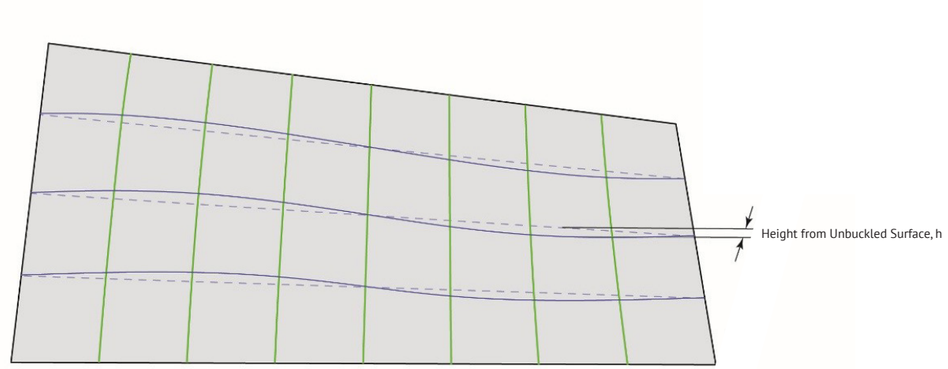

FIGURE 4
Identification of buckling by deviation from unbuckled surface.

FIGURE 5
Photo of buckled glass from previous testing by Enclos.

Research conducted by Enclos Corp. sought to examine the buckling ratio *α* further.[1] The research was conducted on twelve samples of glass of three different thicknesses at four aspect ratios each, as seen in Table 1. Short dimension was held constant, so the effects of thickness were primarily investigated. Each glass sample was structurally glazed to an extruded aluminum frame section and the twisted out of plane. Finite element models for each sample were also constructed as a part of the testing.

The shape of each glass specimen surface was measured with sensitive metrology equipment to confirm the shape at each incremental twist magnitude and to confirm at what magnitude of twist buckling was observed. Finite element models of each specimen were also constructed for this research to simulate the results observed during testing. Displacement of points along the centerlines were measured and used to identify when the measured points deviated from the unbuckled shape. The deviation, *h*, was measured at incremental twist angles and used to identify the onset of buckling, as seen in Figure 4. The buckled surface was apparent upon visual inspection as seen in Figure 5, and could be manipulated by the force of one hand to produce alternate buckled modes.

TEST SETUP

EXPLORATORY MODELING

For the continued research, exploratory finite element models were developed to identify appropriate specimens that would exhibit buckling limits and also exhibit stress limits. Unlike previous models, for this round the variability arising from silicone and frame element stiffness was eliminated; nodes at the perimeter of the model were restrained directly and rigidly forced into the required twisted shape. Stiffer boundary conditions are assumed to generate an upper bound value for achievable twist. The exploratory results indicated that rather than buckling at a constant *α*, the onset of buckling was better described as occurring at a constant value of *k*, as expressed in Eq. (7) below:

(7)

$$k = \left(\frac{d}{t}\right) \cdot \left(\frac{B}{\sqrt{B^2 + L^2}}\right)$$

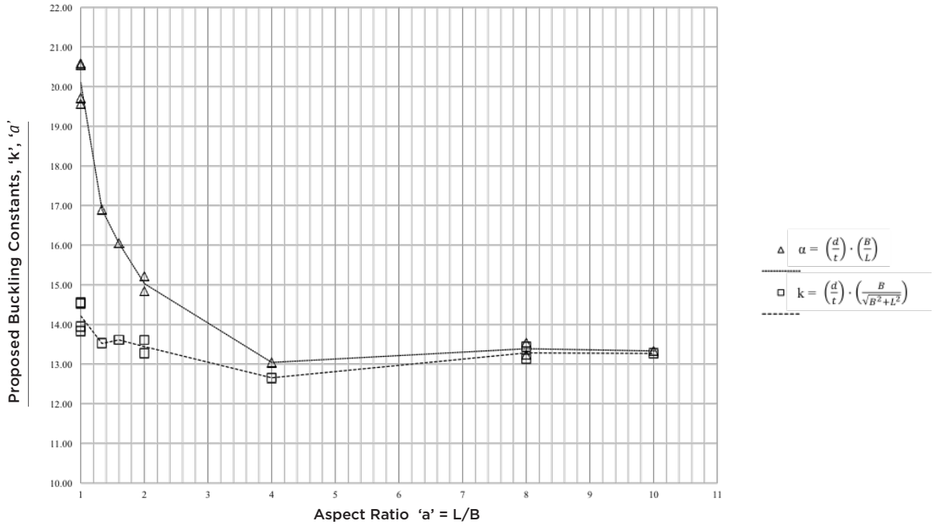

A comparison between the previously expressed ratio, *α*, to the modified ratio, *k*, at the point of buckling in the exploratory finite element analyses confirms the ratio *k* is more consistent predictor of buckling for a range of aspect ratios as seen in Figure 6.

For comparison sake, the experimental and analytical results from the previously conducted Enclos tests were re-analyzed and plotted using the ratio, *k*. The ratio, *k* fits well with the buckling observations from the earlier tests, as seen in Figures 7 and 8.

Expressed in Eq. (9) by introducing the aspect ratio, *a*.

(9)

$$\theta'_{buckling} = \frac{k_{buckling} \cdot \sqrt{(1+a^2)} \cdot t}{B^2 \cdot a}$$

Where aspect ratio, *a*, is:

(10)

$$a = \frac{L}{B}$$

FINITE ELEMENT MODEL APPROACH AND SPECIMEN SELECTION

Based on the buckling predictions discussed, a test plan was developed to investigate maximizing twist. The plan considered a regime of carefully selected specimens that would exhibit buckling at achievable stress levels for tempered glass. Finite element models were then built to identify buckling onset and identify principal stress results at the surface.

FIGURE 6
Investigation of buckling ratio at observed buckling point in preliminary finite element models.

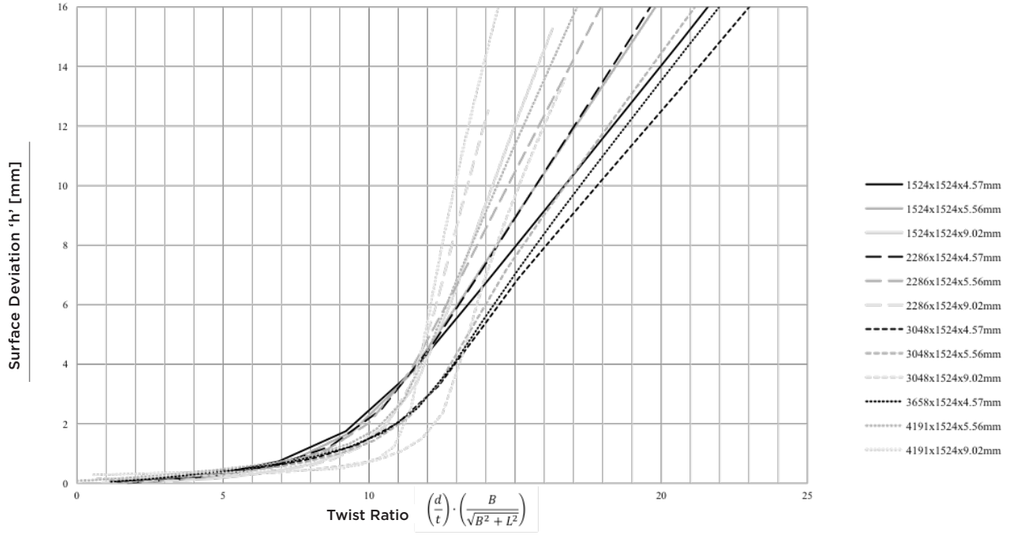

FIGURE 7
Finite element model buckling surface deviation at increasing twist based on ratio, *k*.

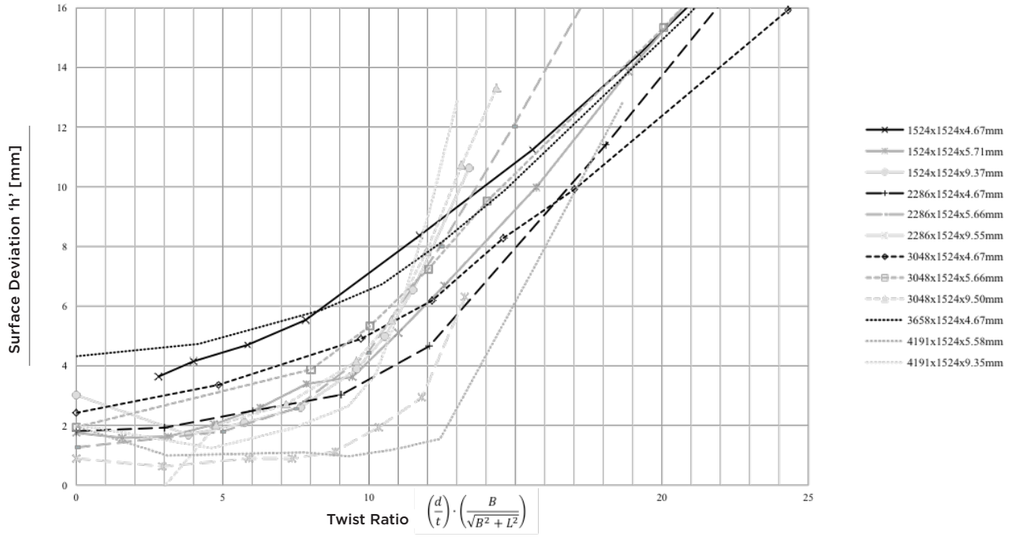

FIGURE 8
Physical test measurements of surface deviation at increasing twist, based on ratio, *k*.

SHORT DIMENSION 'B' [MM]	1ST THICKNESS 'T' IN FEA [MM]	2ND THICKNESS 'T' IN FEA [MM]	3RD THICKNESS 'T' IN FEA [MM]
400	2.16	2.92	--
480	2.16	2.92	--
600	2.16	2.92	3.78
800	2.92	3.78	4.57
1500	5.56	7.42	9.02

TABLE 2
Finite element model specimens for each aspect considered.

DEFORMATION	RATIO 'K'	PERCENTAGE OF $K_{BUCKLING}$ [%]
1	0	0%
2	0.675	5%
3	1.35	10%
4	2.7	20%
5	5.4	40%
6	8.1	60%
7	10.8	80%
8	11.475	85%
9	12.15	90%
10	12.825	95%
11	13.5	100%
12	14.175	105%
13	14.85	110%
14	15.525	115%
15	16.2	120%

TABLE 3
Deformation increments.

The test specimens chosen consisted of a set of five families of finite element models, where each family corresponded to a distinct aspect ratio of long to short dimension. Aspect ratio families modeled were 1:1, 1.2:1, 1.5:1, 2:1 and 5:1. Each aspect family included 13 different combinations of thickness, and short dimension as seen in Table 2.

The models and deformation increments were chosen to identify the onset of buckling with a resolution of +/- 5% of the predicted buckling twist magnitude. As such, the corner displacements for each model were scaled to generate twist increments of consistent magnitude of the ratio, *k*, as seen in Table 3. Deformation increments shown in Table 3 were used in each model based on the specimen dimensions and the anticipated twist at buckling as defined by $k_{buckling}$=13.5. The resulting number of finite element models totaled 65.

RESULTS

BUCKLING

Buckling of the specimens was observed in each of the finite element models. The majority of specimens buckled at the twist deformation increment predicted, where $k_{buckling}$ =13.5. Some specimens exhibited buckling at the deformation increment immediately prior or immediately following the predicted increment as seen in Figure 9. Thus, buckling was observed for values of *k* varying from 12.825 to 14.175 based on the deformation increments identified in Table 3. The higher values of *k* at buckling were observed at the 1:1 aspect ratios, which is also consistent with Figure 6. This indicates that there may yet remain a better constant ratio to predict buckling. Regardless, for this research buckling was predicted for the finite element models to +/-5% using $k_{buckling}$=13.5.

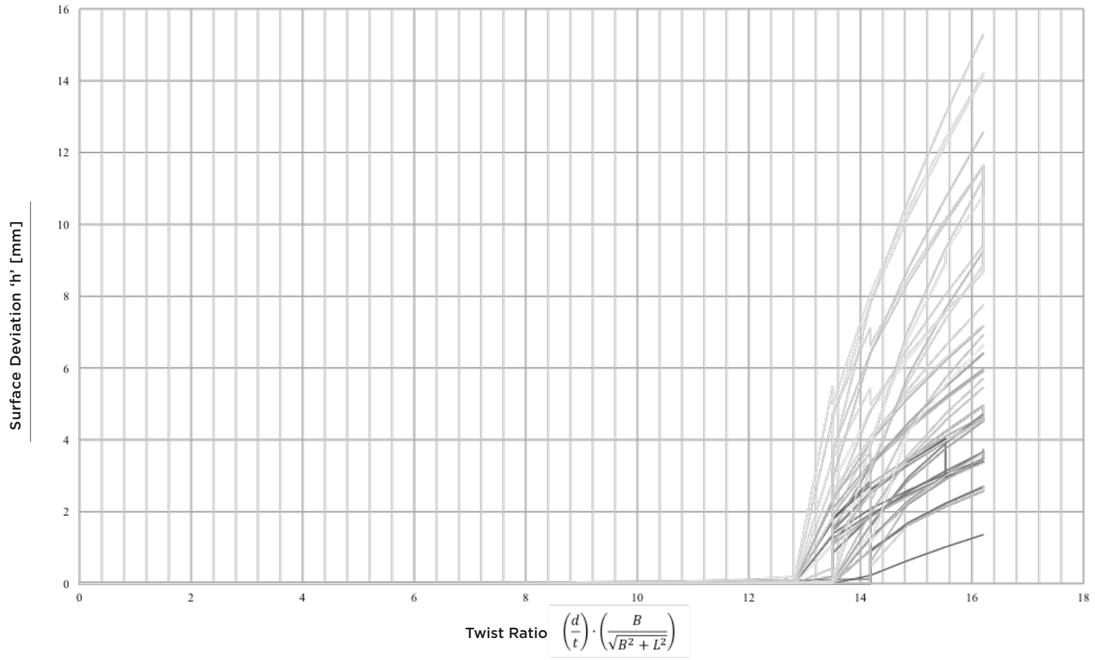

FIGURE 9
Buckling observations for all finite element models.

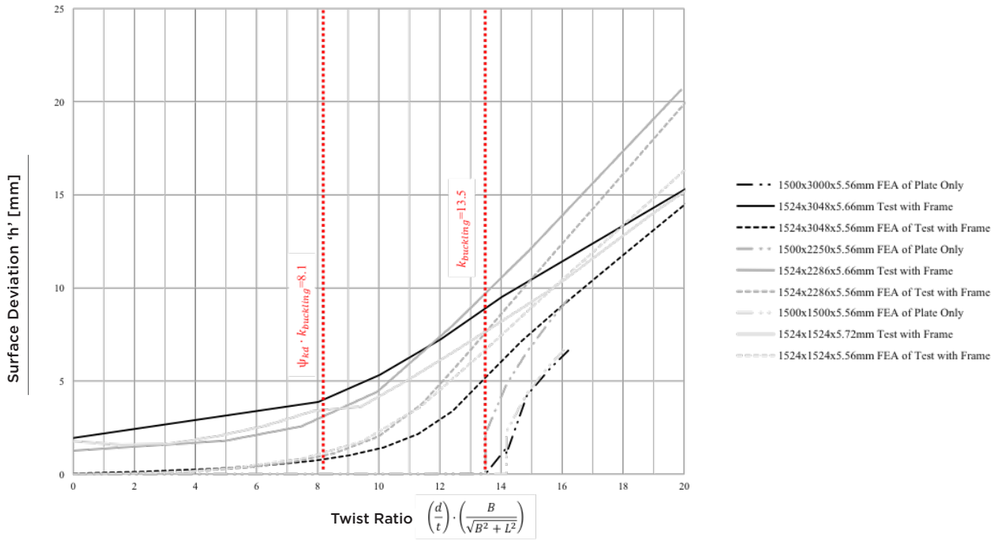

FIGURE 10
Buckling comparison to previous finite element analysis and physical test at 5.56 mm.

The buckling results were then compared to the previous test results and physical testing in Figure 10 and 11 to quantify a knockdown factor appropriate for the specimens tested previously. As evident from Figure 10 and 11, a knockdown factor, ψ_{kd}, of roughly 0.6 times the theoretical $k_{buckling}$ is considered based on a visual review of the physical test results in comparison to the ideal specimen models. The result is that the ideal $k_{buckling}$ = 13.5 is reduced to a value of $k_{buckling}$ = 8.1. Of course for design, an adequate safety factor Ω to buckling also would be included, as shown in Eq. (11):

(11)

$$\theta'_{buckling\_allowed} = \frac{\psi_{kd} \cdot k_{buckling} \cdot \sqrt{\left(1+a^2\right)} \cdot t}{\Omega \cdot B^2 \cdot a}$$

Thus, Eq. (11) considers a knockdown factor, ψ_{kd}, and a safety factor, Ω, to modify Eq. (9) for avoiding buckling in engineering practice.

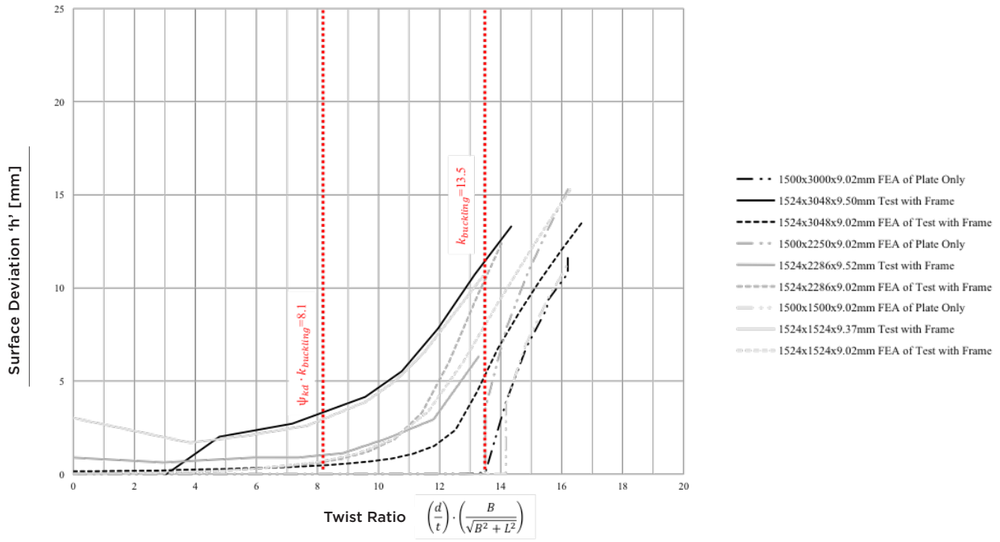

FIGURE 11
Buckling comparison to previous finite element analysis and physical test at 9.02 mm.

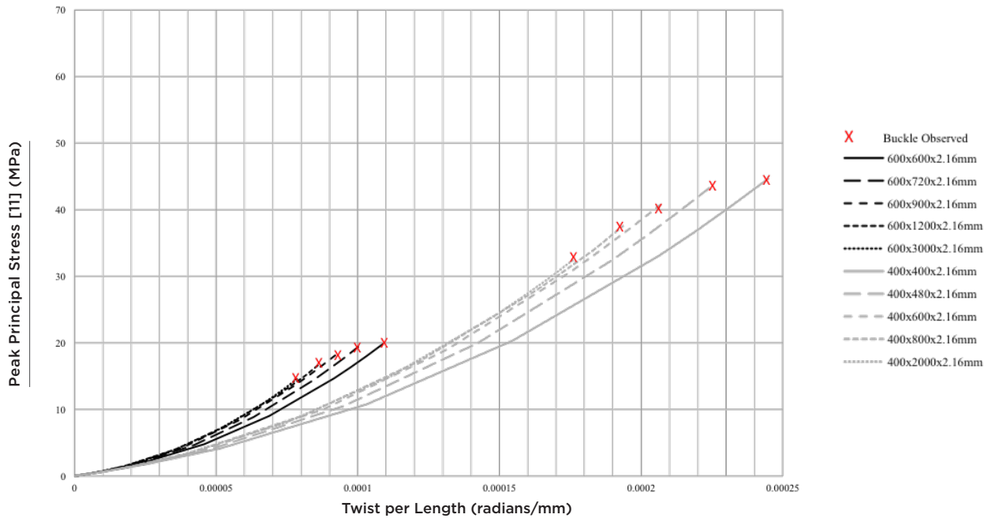

STRESSES

Determination of peak principal stress is required for comparison to glass capacity. As a result, maximum principal stresses in tension from the finite element models were compiled into a spreadsheet for each of the finite element models. The peak principal stresses were plotted by aspect ratio family for the specimens with *a*=1 and *a*=5 over a range of twist increments, as seen in Figures 12 and 13 respectively. These plots do not include the effects of any transverse pressure.

The increment where *k*=13.5 was chosen as the final point on all the plots, although data does exist beyond that increment. However, the stresses beyond the point of buckling do not follow the same trend as observed below the twist at buckling. Ending the plots at *k*=13.5 also provided a convenient way to reveal the buckling relationship on the same plot as the stresses. The twist magnitude at buckling is found at the end point of each stress curve plotted, denoted with an 'X' mark in the plots.

There are several trends that merit discussion. First, reducing the short dimension greatly impacts the magnitude of twist that is achievable, as seen in Figures 12 and 13. Second, increased thickness increases resistance to buckling. Third, increasing the thickness does increase the stress when transverse pressure is not considered, although it is a relatively minor increase compared to the benefit to buckling resistance. Finally, as seen in Figure 14 an increase in aspect ratio reduces the buckling resistance and increases the stress. However, as the aspect ratio increases, the negative effects on buckling resistance and stress appear to converge to a single curve for a given short dimension and thickness.

Thus, an aspect ratio of unity yields the optimal ability to achieve twist, by maximizing buckling stability and minimizing principal stresses arising from twisting the glass. Likewise, achievable twist decreases for increasing aspect ratios, but converges on a limit that is noticeably lower.

FIGURE 12
Plate stresses and buckling from twisting without transverse load (1:1 Aspect).

FIGURE 13
Plate stresses and buckling from twisting without transverse load (5:1 Aspect).

FIGURE 14
Comparison for buckling and stress with no transverse load p=0kPa at t = 2.16mm, B = 400mm and B = 600mm.

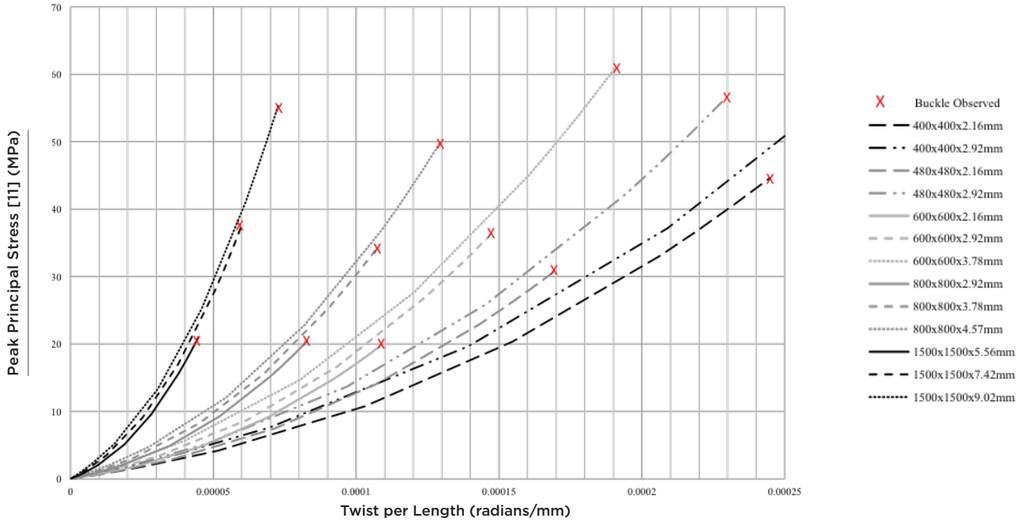

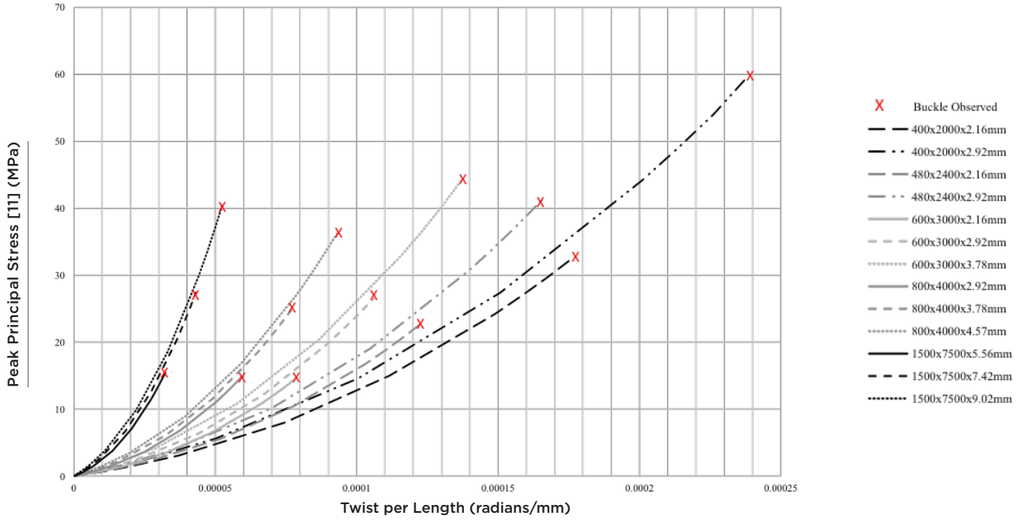

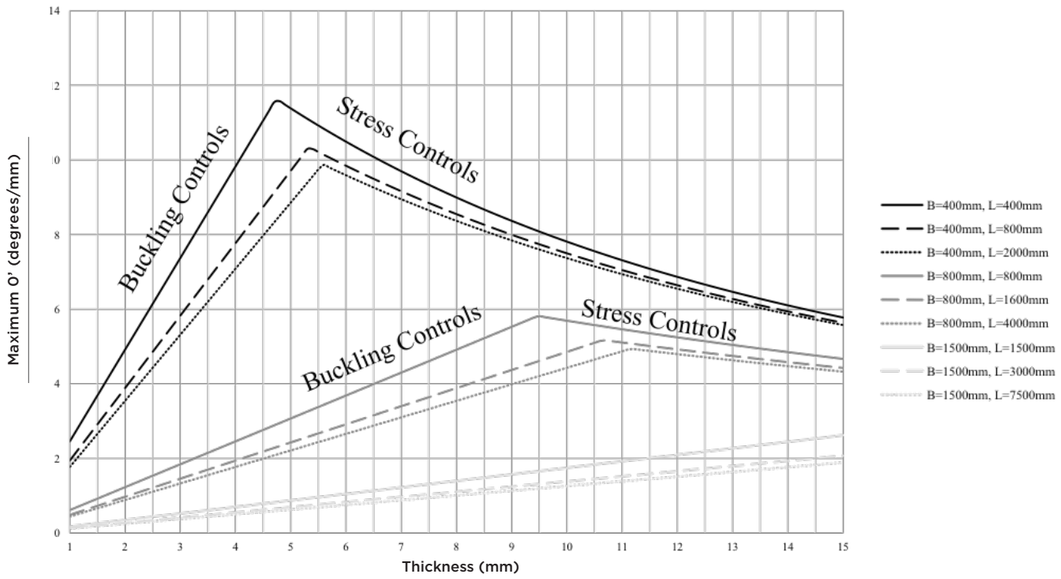

Analysis of peak principal stresses due to twisting yielded an approximation that seems to fit the data empirically. This expression is given in Eq. (12), based on a shear modulus of G=28.9GPa:

(12)

$$\sigma_{11} = \theta' \cdot G \cdot t \cdot \left[1 + \frac{1}{c} \cdot \left(\frac{\theta'}{t} \cdot \frac{B^2 \cdot L}{\sqrt{B^2 + L^2}} \right) \right]$$

A new constant, c≈6.4, was introduced empirically to fit the results from the finite element model within approximately +/-5% of the peak principal stress values.

Eq. (12) can be simplified into the quadratic shown in Eq. (13) below:

(13)

$$\sigma_{11} = \theta'^2 \cdot \left(\frac{G}{c} \cdot \frac{B^2 \cdot a}{\sqrt{1 + a^2}} \right) + \theta' \cdot t \cdot G$$

Solving the quadratic Eq. (13) for achievable twist as a function of allowed principal stress, $\sigma_{11allowed}$ gives Eq. (14):

(14)

$$\theta'_{stress} = \frac{-t \cdot G + \sqrt{t^2 \cdot G^2 + \frac{4 \cdot \sigma_{11allowed} \cdot a \cdot B^2 \cdot G}{c \cdot \sqrt{1 + a^2}}}}{\frac{2 \cdot a \cdot B^2 \cdot G}{c \cdot \sqrt{1 + a^2}}}$$

FIGURE 15
Maximum achievable twist for various short dimensions controlled by buckling and stress.

FINDING THE MAXIMUM OF DIFFERENTIAL TWIST

The objective of this research is to maximize differential twist, θ'. Note that the limiting differential twist functions controlled by buckling and stress are defined reasonably well in algebraic formulas in Eq. (11) and Eq. (14), respectively. For aspect ratio a=1, Eq. (11) is simplified to the relationship in Eq. (15) for achievable differential twist without buckling on a square lite:

(15)

$$\theta'_{buckling\_allowed\_square} = \frac{\psi_{kd} \cdot k_{buckling} \cdot \sqrt{2} \cdot t}{\Omega \cdot B^2}$$

As Eq. (11) is evaluated for ever increasing aspect ratios, it is seen that:

(16)

$$\lim_{a \to \infty} \theta'_{buckling\_allowed} = \frac{\psi_{kd} \cdot k_{buckling} \cdot t}{\Omega \cdot B^2}$$

The same simplifications can be prepared for the stress equations. For aspect ratio a=1, Eq. (14) is simplified to the relationship in Eq. (17) for achievable differential twist without overstressing a square lite:

(17)

$$\theta'_{stress\_square} = \frac{-t \cdot G + \sqrt{t^2 \cdot G^2 + \frac{4 \cdot \sigma_{11allowed} \cdot B^2 \cdot G}{c \cdot \sqrt{2}}}}{\frac{2 \cdot B^2 \cdot G}{c \cdot \sqrt{2}}}$$

As Eq. (14) is evaluated for ever increasing aspect ratio, a, it is seen that:

(18)

$$\lim_{a \to \infty} \theta'_{stress} = \frac{-t \cdot G + \sqrt{t^2 \cdot G^2 + \frac{4 \cdot \sigma_{11allowed} \cdot B^2 \cdot G}{c}}}{\frac{2 \cdot B^2 \cdot G}{c}}$$

The remaining unknowns are the appropriate safety factor to buckling and the appropriate allowable principal stress for long duration load. For the purposes of this report, a safety factor to buckling of Ω=1.67, and a knockdown factor to buckling of ψ_{kd}=0.6 will be used. No claim is made that these factors are adequate for engineering purposes. Rather, they are assumed for the purposes of a qualitative discussion.

Just as a knockdown factor and a safety factor are needed to avoid buckling risk, glass capacity will also need to be limited to a safe level. For the purposes of this paper, an allowable stress at long duration, $\sigma_{11allowed}$ = 48.9MPa is used.

Maximum acceptable twist as limited by buckling and strength functions may then be plotted on one graph using the minimums from the buckling and stress limit functions for any combination of thickness, length, and width dimensions as seen in Figure 15.

These formulas can also be conveyed as contour lines of achievable differential twist given ordinates of short dimension and thickness as seen in Figure 16. In fact, Figures 15 and 16 convey cross section cuts and contour lines from the surface of the optimal twist function, shown for the aspect ratio a=1 in Figure 17. Essentially, Figure 17 shows a surface with two facets. One facet is over the domain where buckling controls the ability to twist, the other facet is over the domain where stress controls the ability to twist.

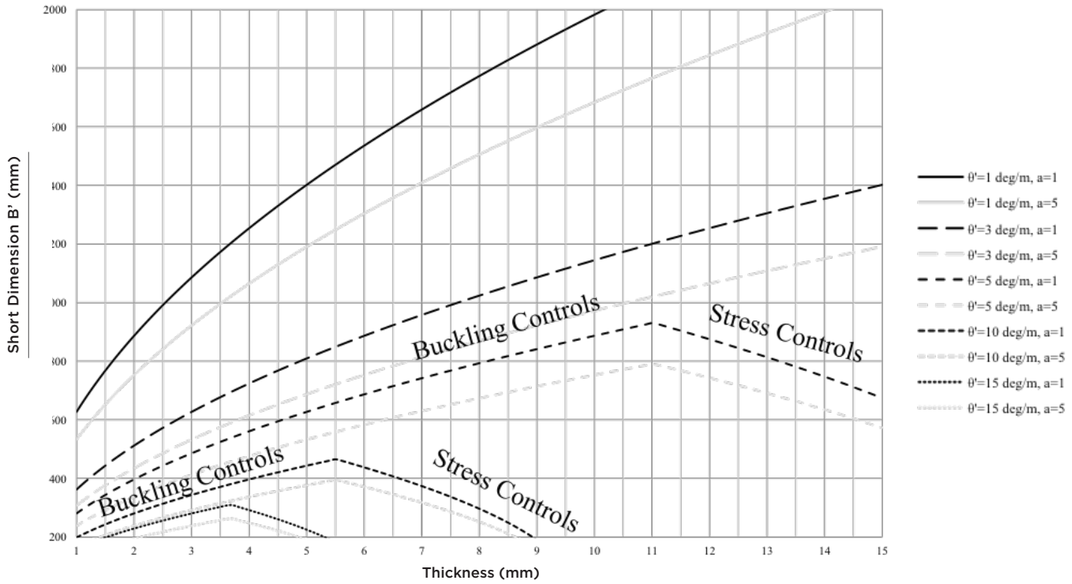

CONCLUSIONS

As a result of this study, the twist magnitude at the onset of buckling is predicted and appears consistent with prior physical testing and finite element modeling. The magnitude of principal stress resulting from the torsional case considered is also predicted with a formula that approximates the finite element results. These are both expressed with algebraic functions that can be plotted to find the maximums.

In terms of application, the greatest differential twist magnitudes are achieved by first selecting the smallest short dimension that is acceptable to meet the project requirements. Aspect ratios as close to unity as possible are also beneficial to maximizing twist per length. However, the aspect ratio is limited in its impact, whether beneficial or detrimental. After selecting an appropriate short dimension and aspect ratio, thickness selection should be made to avoid buckling and avoid excessive stress from twisting. Ultimately, proper engineering practice would dictate design load cases also be considered in combination with the stresses arising from the forming operation.

If the desired magnitude of twist is known or specified, the results presented in this paper can also be applied to determine the optimal combination of short dimension, thickness, and aspect ratio to achieve the desired magnitude of twisting. Of course, the optimal combination is dependent on the appropriate knockdown and buckling safety factors and glass capacity determination. Along these lines, additional research will be required to determine appropriate values of $k_{buckling}$, c, Ω, and ψ_{kd} as presented in this paper. More research is also needed to confirm the buckling ratio k is the best fit to predict the onset of buckling. Glass that is trapezoidal, parallelogram, and other non-orthogonal shapes will also need to be researched to continue the advancement of this topic.

Regardless, the results presented in this paper are expected to advance the achievable magnitude of twist of cold warped glazing in architectural applications. Twist angles many times greater than previously achieved are definitely within reach by using proper selection of thickness and short dimension. As a result, the possibilities are endless to create exciting, bold, and breathtaking designs that have never been realized before.

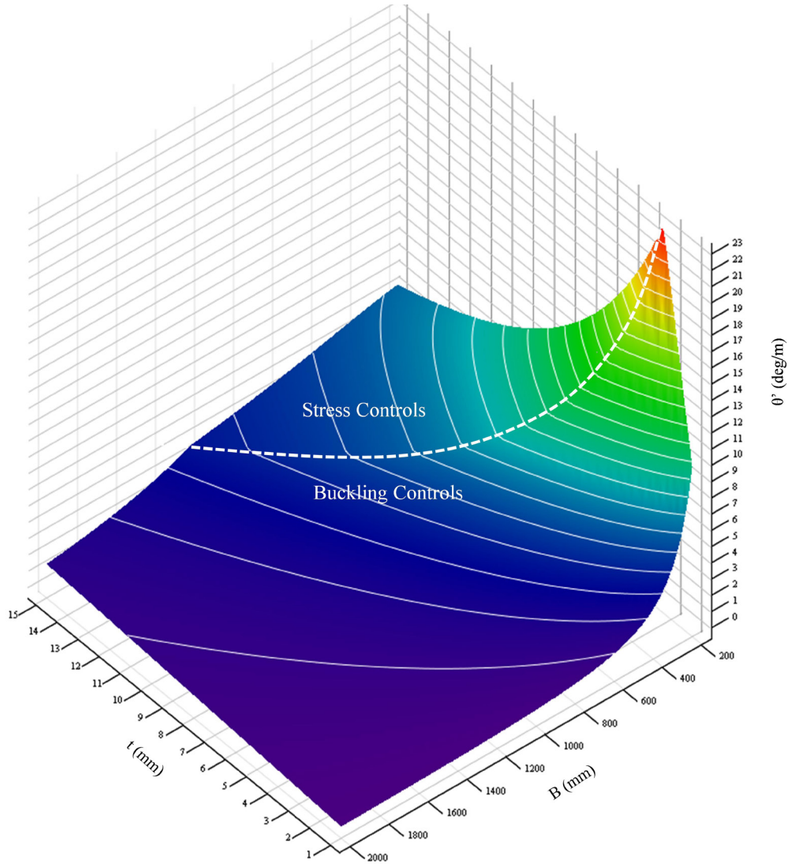

FIGURE 16
Contours of maximum differential twist allowed per short dimensions and thickness.

FIGURE 17
Surface plot of the *θ'* function limited by stress buckling for aspect ratio α=1.

MAXIMIZING THE TWIST OF COLD FORMED GLAZING

[0] *This article is an adaption of the Challenging Glass 5 - Conference on Architectural and Structural Applications of Glass paper of the same title presented by the author in June 2016 at Ghent University in Belgium.*

[1] ASTM Standard E1300-12a$^{\varepsilon 1}$: Standard practice for determining load resistance of glass buildings. In: Annual Book of ASTM Standards, ASTM International, West Conshohocken, PA. (2012)

[2] Bensend, A.: Beneath the surface: buckling of cold formed glass. In: Glass Performance Days 2015 Conference Proceedings, pp. 241-246, Glass Performance Days, Tampere, 24-26 June 2015

[3] Benson, R.C., and Crispino, D.J.: Stability of twisted orthotropic plates. Int. J. Mech. Sci. 28(6), 371-379 (1986)

[4] Besserud, K., Bergers, M., Black, A.J., Carbary, L.D., Misson, D., and Rubis, K.: Durability of cold-bent insulating-glass units. Journal of ASTM International (JAI), 9(3), 205-242 (2012). doi:10.1520/JAI104120

[5] Carter, C.J., and Seaburg, P.A.: Torsional analysis of structural steel members: Steel design guide series 9. AISC, USA (1997)

[6] Eekhout, M., Staaks, D., and Van Herwijnen, F.: Cold bent glass sheets in facade structures. Structural Engineering International (SEI), 14(2), 98-101 (2004)

[7] Galuppi, L., Massimiani, S., Royer-Carfagni, G.: Buckling phenomena in double curved cold-bent glass. Int. J. Nonlin. Mech. 64, 70-84 (2014). doi: 10.1016/j.ijnonlinmec.2014.03.015

[8] Green, A.E.: The equilibrium and elastic stability of a thin twisted strip. Proc. R. Soc. Lon. Ser.-A. 125, 430-455 (1936). doi: 10.1098/rspa.1936.0061

[9] Green, A.E.: The elastic stability of a thin twisted strip—II. Proc. R. Soc. Lon. Ser.-A 161, 197-200 (1937). doi: 10.1098/rspa.1937.0141

[10] Hoogenboom, P.C.J.: SEI discussion on paper: Cold bent glass sheets in façade structures. Structural Engineering International (SEI), 14(4), 322 (2004)

[11] Staaks, D.: Koud torderen van glaspanelen in blobs. Thesis, TU Eindhoven, Netherlands (2003)

[12] Van Laar, H.: Stabiliteit van in het werk vervormde glaspanelen voor dubbelgekromde gevels. Thesis, TU Delft, Netherlands (2004)